Structure and Upconversion Luminescence of Hydrothermal $PbWO_4$:Er^{3+}, Yb^{3+} Powders

Qilin Dai,[†] Hongwei Song,*[,‡] Xinguang Ren,[†] Shaozhe Lu,[†] Guohui Pan,[†] Xue Bai,[‡] Biao Dong,[‡] Ruifei Qin,[†] Xuesong Qu,[†] and Hui Zhang[†]

Key Laboratory of Excited State Physics, Changchun Institute of Optics, Fine Mechanics and Physics, Chinese Academy of Sciences, and Graduate School of Chinese Academy of Sciences, 16 Eastern Nan-Hu Road, Changchun 130033, P. R. China, and State Key Laboratory of Integral Optoelectronics, College of Electronic Science and Engineering, JiLin University, Changchun 130012, P. R. China

Received: June 23, 2008; Revised Manuscript Received: September 22, 2008

$PbWO_4$: Er^{3+},Yb^{3+} nanocrystals (~100 nm) were prepared by the hydrothermal method at different pH values (pH = 4, 7, and 9). Their structure and luminescence properties under 978-nm laser-diode excitation were studied. The results indicate that the practical ratio of W to Pb in the nanocrystals and the doping concentration of Yb^{3+} depended strongly on the pH value due to structure change. In upconversion, red ($^4F_{9/2}\rightarrow{}^4I_{15/2}$) and green ($^2H_{11/2}$,$^4S_{3/2}\rightarrow{}^4I_{15/2}$) emissions were observed, both of which occurred via a two-photon populating process. Biexponential upconversion dynamics were observed, which was attributed to luminescence centers surrounded by different local environments. The intensity ratio of $^2H_{11/2}\rightarrow{}^4I_{15/2}$ to$^4S_{3/2}\rightarrow{}^4I_{15/2}$ (R_{HS}) was explored to reveal the local thermal effect under the exposure of the laser diode, showing that the temperature at the exposed spot increased linearly with respect to excitation power density and Yb^{3+} concentration.

I. Introduction

Considerable interest has been centered on the conversion of infrared radiation to shorter wavelength by materials doped with trivalent rare-earth (RE) ions.[1,2] Up to now, various upconversion (UC) host materials have been developed and studied, such as crystals, glasses, ceramics, and so on.[3−5] Recently, the studies on UC luminescence properties of rare-earth (RE) doped nanosized phosphors are attracting interest, because they are significant not only for applications but also for essential understanding of nanocrystal, such as confinement effect, surface effect, etc. In RE-doped nanocrystals, some novel UC properties were observed, such as different population channels in comparison to the bulk, strong saturation effect and local thermal effect, and so on. [6−9] Host materials are important for the UC luminescence. In order to obtain efficient UC phosphors, host materials with lower phonon energies are required; therefore, rare earth doped fluoride nanocrystals have been widely studied because of their low phonon thresholds. However, their physical properties such as chemical stability and mechanical strength are not as good as oxide hosts. Therefore, it is also significant to search for oxide host materials with efficient UC luminescence. Some literature on the UC luminescence of RE-doped oxide nanocrystals such as ZrO_2,Ln_2O_3 (Ln = La, Y, Gd) have been reported.[10−13]

Tungstate is a very important family of oxide materials that have potential application in various fields, such as photoluminescence,[14] microwave applications,[15] optical fibers,[16] and scintillator materials.[17] As a self-activating phosphor, tungstate has some advantages, e.g. high chemical stability, high X-ray absorption coefficient, high light yield, and low afterglow to luminescence.[18] There exist two types of structure in tungstates: wolframite and scheelite. Lead tungstate ($PbWO_4$) has the scheelite structure, and it has been attracting increasing attention because of its technological importance as an inorganic scintillating crystal. $PbWO_4$ has high density (8.3 g/cm^3), high irradiation damage resistance, interesting excitonic luminescence, thermoluminescence, and stimulated Raman scattering behavior.[19,20] Among oxide materials, its phonon threshold is relatively low. In addition, compared with the other Er^{3+}-doped materials, in $PbWO_4$ matrices, W ions with larger electric charge and small radius have strong polarization, consequently decrease symmetries, and enhance stark energy splitting of Er^{3+} ions in the crystal field.[21] We expect that $PbWO_4$ could act as an efficient host for UC luminescence. Here, we present the hydrothermal preparation, structure, and UC luminescence properties of $PbWO_4$:Yb^{3+}, Er^{3+} nanocrystals. The Er^{3+} ion has a favorable energy level capable of ~978-nm infrared pumping. There is a large spectral overlap between the $^2F_{5/2}-{}^2F_{7/2}$ Yb^{3+} NIR emission and the $^4I_{11/2}-{}^4I_{15/2}$ Er^{3+} absorption bands, which results in an efficient energy transfer from Yb^{3+} to Er^{3+}. The UC luminescence properties in different hosts have frequently been studied; however, the UC luminescence of rare-earth-doped $PbWO_4$ has not been studied, to our knowledge.

In this paper, the influence of pH value on nanocrystalline structure, the local thermal effect induced by laser exposure, and the biexponential UC dynamics were the focus.

II. Experimental Section

A. Sample Preparation. Lead tungstate ($PbWO_4$) nanocrystals were prepared by the reaction of $Pb(NO_3)_2$, $Yb(NO_3)_3$, and $Er(NO_3)_3$ as well as Na_2WO_4 for 12 h at a certain temperature (160 °C) and different pH values. In a typical procedure, $Yb(NO_3)_3\cdot5H_2O$, $Er(NO_3)_3\cdot5H_2O$, $Pb(NO_3)_2\cdot5H_2O$, and $Na_2WO_4\cdot2H_2O$ were dissolved in deionized water, respectively. Then the former three solutions were mixed together [1 mmol $Pb(NO_3)_2$, 0.1 mmol $Yb(NO_3)_3$ and 0.01 mmol $Er(NO_3)_3$], and then appropriate Na_2WO_4(1 mmol) was added with vigorous stirring. The pH value (pH = 4, 7, 9) of the mixed solution was adjusted with dropwise addition of HNO_3 or NaOH solution.

* Corresponding author. Fax: 86-431-86176320. E-mail: hwsong2005@yahoo.com.cn.
[†] Chinese Academy of Sciences, and Graduate School of Chinese Academy of Sciences.
[‡] JiLin University.

10.1021/jp805587q CCC: $40.75
Published on Web 11/13/2008

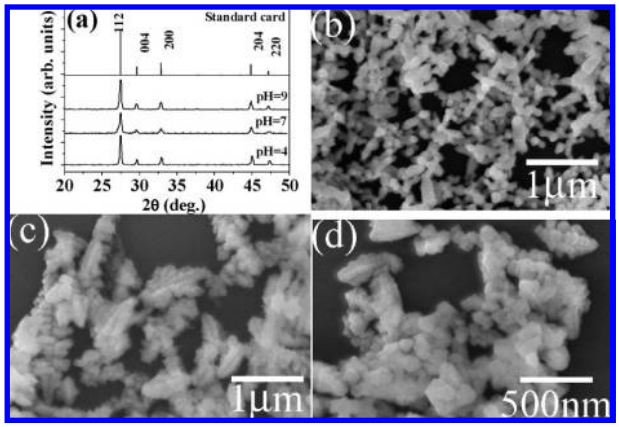

Figure 1. (a) XRD patterns of $PbWO_4:Er^{3+}$, Yb^{3+} nanopowders prepared under different pH values. FE-SEM images of the (b) pH = 4, (c) pH = 7, and (d) pH = 9 samples.

After that, the solution was added into a Teflon-lined stainless steel autoclave of 50.0 mL capacity. The autoclave was kept at 160 °C for 12 h. Afterward, the autoclave was cooled to room temperature gradually. Then the white precipitate was collected and washed with deionzed water several times. The solid was heated at 80 °C and dried under vacuum for 2 h; finally, the white powders of $PbWO_4$: Er^{3+}, Yb^{3+} (the doping concentration was 10 mol % Yb^{3+}, 1 mol % Er^{3+}) were obtained. We also prepared different Yb concentration samples with the above method.

B. Measurements. Field emission scanning electron microscopy (FE-SEM) was taken on a Hitachi S-4800 electron microscope. X-ray diffraction (XRD) data were collected on a Rigaku D/max-rA X-ray diffractometer using a Cu target radiation source. The FTIR absorption spectra were measured by a FTS3000 FTIR spectrometer. In the measurements of UCL emission spectra, a continuous 978-nm diode laser with power maximum of 2 W was used for excitation, with a focused area of 0.25 mm^2. The visible emissions were collected using an F-4500 spectrometer. The element analysis was performed on a Leeman prodigy inductively coupled plasma atomic emission spectrometer (ICP-AES). In the measurement of luminescence dynamics, a 978-nm pulsed light (10 ns duration) originating from the optical parameter oscillator (OPO) laser was used as excitation source.

III. Results and Discussion

A. Influence of pH Value on Structure of $PbWO_4$. First, the nanocrystalline structure and profile of the $PbWO_4$ hydrothermal products were characterized. Figure 1a shows the XRD patterns of the samples prepared at different pH values and the standard card, and Figure 1b−d shows the FE-SEM images of them. From Figure 1a it can be seen that all the nanocrystals are pure tetragonal in phase (JCPDS No. 85-1857). The detailed origins of the XRD peaks are labeled in the figure. From the SEM images, the hydrothermal products prepared at different pH values are all club-shaped nanoparticles. The diameters of the nanoparticles are about 100 nm and the lengths are about 200−300 nm. The nanoparticles tend to aggregate together, especially for the pH = 7 and 10 samples. The pH value does not influence the size of the nanocrystals much.

FTIR spectra were measured, as shown in Figure 2. According to the literature, the absorption band around 700−900 cm^{-1} was ascribed to the W−O stretching vibration in WO_4 tetrahedron.[22,23] The bands at ∼1625 and ∼3500 cm^{-1} are assigned to the OH^- bending and stretching modes, respectively. The bands at ∼1450 cm^{-1} in the pH = 7 and 9 samples are assigned to the vibration of CO_3^{2-}. The existence of OH^- and CO_3^{2-} bonds implies the surface adsorption of CO_3^{2-} and water. In comparison to the typical vibration of WO_4^{2-}, the vibration strength of the OH^- and CO_3^{2-} is not high, implying that the surface adsorption is less.

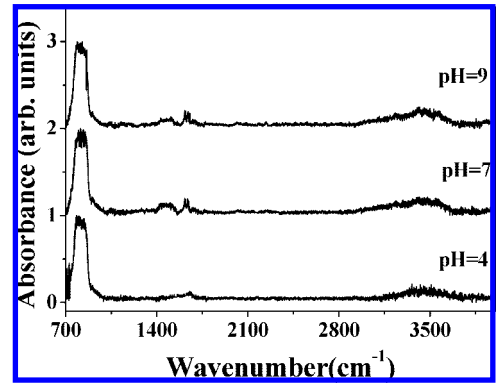

Figure 2. The FTIR spectra for the different samples.

TABLE 1: ICP Results of Different Samples: Molar Ratio of W to Pb and Content of Er^{3+} and Yb^{3+}

	pH = 4	pH = 7	pH = 9
molar ratio W:Pb	1:1.09	1:1.17	1:1.18
Er^{3+} content (mol %)	0.51	0.51	0.53
Yb^{3+} content (mol %)	1.42	2.22	3.79

The results of element content analysis by ICP-AES are listed in Table 1. Yb and Er are respectively 1.42% and 0.51% for the pH = 4 sample, 2.22% and 0.51% for the pH = 7 sample, and 3.79% and 0.53% for the pH = 9 sample. This indicates that a high pH value benefits efficient doping of Yb^{3+}. It can also be seen that the molar ratios of the W to Pb are 1:1.09, 1:1.17, and 1:1.18 in pH = 4, 7, and 9 samples. This indicates that Pb element is excessive for all three samples, and this tendency is more obvious in the pH = 9 sample. The precursor solution for the pH = 9 contains much OH^-, while that for pH = 4 contains less. It is suggested that some Pb^{2+} could combine with OH^- groups in the solution, forming $Pb(OH)_2$ on the surface of the nanoparticles. However, $Pb(OH)_2$ are not identified by the XRD patterns, indicating that if the $Pb(OH)_2$ really exists, it should be noncrystalline. Similar results have been reported in other materials.[24] It is natural that in the pH = 9 solution more $Pb(OH)_2$ is formed. According to the ref 25, rare earths can substitute for both Pb^{2+} and W^{6+} in the $PbWO_4$ host. The present results suggest that Yb^{3+} prefers to substitute for W^{6+}.

B. Upconversion Luminescence Spectra and Power Dependence. Figure 3a,b shows the UC spectra of the different nanocrystals under the 978-nm excitation. In the spectra, the green emissions were observed in the range of 500−580 nm, corresponding to the $^2H_{11/2}/^4S_{3/2}-^4I_{15/2}$ transitions, while the red lines were observed between 640 and 690 nm, corresponding to the $^4F_{9/2}-^4I_{15/2}$ ones. It is interesting to observe that the intensity ratio of $^2H_{11/2}\rightarrow{}^4I_{15/2}$ to $^4S_{3/2}\rightarrow{}^4I_{15/2}$ in the pH = 4 sample is smaller than that in the pH = 9 sample. This will be discussed in the later section. Figure 3c depicts the dependence of UC intensity on excitation power in log−log plots for different pH samples. It can be seen that as the pump power I_{IR} was lower than 0.5 W, the emission intensity I_v increased with I_{IR} obeying the rule $I_v \propto I_{IR}^n$. As the power surpassed 0.5 W, I_v tended to decrease, which can be explained by the "saturation" process and thermal effect.[6] In the figure, the slopes for different samples

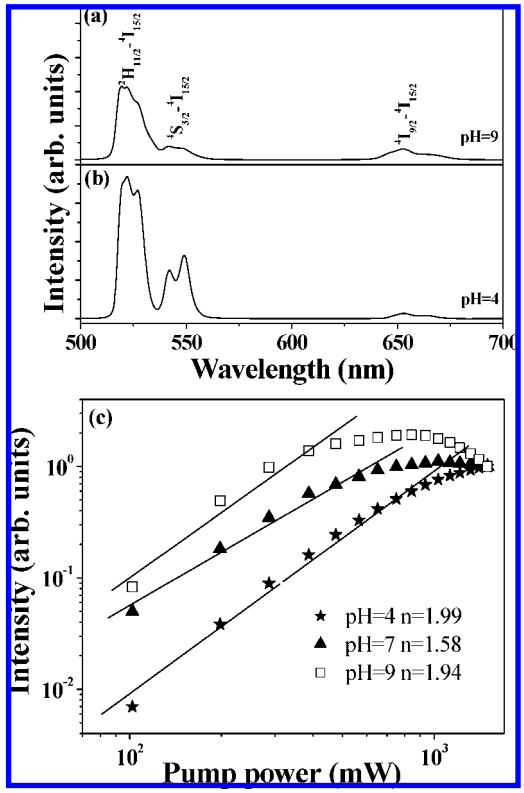

Figure 3. (a, b) Upconversion luminescent spectra of the different $PbWO_4$:1% Er^{3+}, 10% Yb^{3+} nanocrystals (prepared at different pH values) under the 978-nm excitation with different powers. (c) $\log_{10}-\log_{10}$ plot of emission intensity as a function of excitation power for different samples.

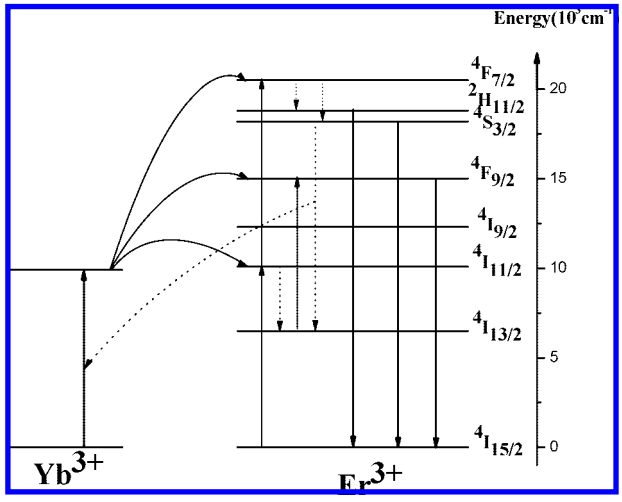

Figure 4. the UC luminescence mechanism and population processes.

are determined to be $n = 1.99$, 1.58, and 1.94, respectively, for the pH = 4, 7, and 10 samples. A slope equal to approximately 2 indicates that upconversion occurs via a two-photon process. Note that the slope of 2 is due to a sequential absorption process and not a two-photon absorption one.

The UC luminescence mechanism and population processes in Er^{3+}/Yb^{3+}-codoped systems are presented in Figure 4, which have been frequently described in other references.[6,7,26] First, the Er^{3+} ion is excited from the ground state $^4I_{15/2}$ to the excited state $^4I_{11/2}$. Subsequent nonradiative relaxations of $^4I_{11/2} \rightarrow {}^4I_{13/2}$ also populate the $^4I_{13/2}$ level. In the second-step excitation, the excited-state atoms are excited from the $^4I_{11/2}$ to the $^4F_{7/2}$ levels

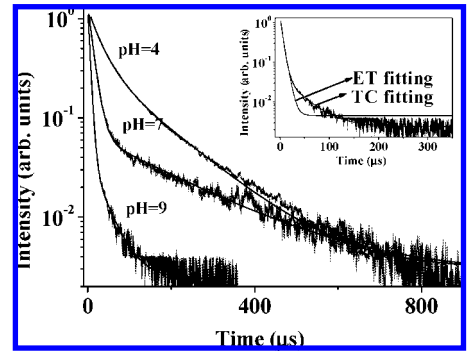

Figure 5. (a) Fluorescence decay curves in different samples, monitoring at 520 nm; the scattered dots are experimental data and solid lines are fitting curves. Inset: the decay curves for pH = 9 sample fitted by energy transfer model (ET) and by biexponential model (BE).

or from the $^4I_{13/2}$ to $^4F_{9/2}$ states. The populated $^4F_{7/2}$ may mostly nonradiatively relax to $^2H_{11/2}$ and $^4S_{3/2}$ levels, which produce two green upconversion emissions. The populated $^4F_{9/2}$ level causes red emissions.

C. Biexponential Upconversion Dynamics. Figure 5 shows the fluorescence decay curves in different pH samples, monitoring at 520 nm. From the experimental curves, the emissions for the green level at 520 nm decay nonexponentially. We consider that there exist two main possibilities, which can lead to nonexponential UC dynamics for the green emissions of Er^{3+}. First, there exists considerable back energy transfer from the green level of Er^{3+} to Yb^{3+}. Second, there exist two or several different Er^{3+} centers and their luminescence dynamics are different. Therefore, we fitted the experimental data with two different functions, the function based on energy transfer, which can be written as[27]

$$I(t) = I(0)\exp[(-t/\tau_R) - (t^{3/n}/\tau_{3/n})] \quad (1)$$

with

$$1/\tau_{3/n} = \frac{4\pi}{3} n_D \Gamma\left(1 - \frac{3}{n}\right) R_{min}{}^3 (W_{0l})^{3/n} f_{BT} \quad (2)$$

where τ_R is the intrinsic decay time of the excited Er^{3+} ions, n_D is the density of donors, $n = 6$, 8, 10 for dipole−dipole, dipole−quadrupole, and quadrupole-quadrupole mechanisms, R_{min} is the closest distance between nearest neighbor cations, and W_{0l} is the transfer rate between Er^{3+} ions in nearest-neighbor sites. f_{BT} is a factor to take back-transfer into account.

The biexponential function based on two different centers can be written as

$$I = R_1 e^{-t/\tau_1} + R_2 e^{-t/\tau_2} \quad (3)$$

where τ_1 and τ_2 represent the faster and slower decay time constants and R_1 and R_2 are corresponding contributions of the faster and the slower component, respectively. The fitting results by different models for the pH = 9 sample are drawn in the inset of Figure 5. It can be seen that the energy transfer model (ET) can not well fit the experimental data, while the two-center model (TC) can exactly fit the data. Therefore, we suggest that the nonexponential dynamics are contributed by two different luminescent Er^{3+} centers. In Figure 5, all the experimental dynamics are well fitted by the two-center model. The pH = 9 samples doped with different Yb content were also measured. The fitting lifetimes of all samples are shown in Table 2. It can be seen that both the longer and the shorter lifetime decreased greatly with Yb content, which was consistent with our previous

TABLE 2: Decay Time Constant of Er^{3+} in Different Samples, with Monitoring at 520 nm[a]

samples	τ_1 (μs)	R_1 (%)	τ_2 (μs)	R_2 (%)
pH = 4, 10%	124.9 ± 0.3	28.9	28.8 ± 0.6	71.1
pH = 7, 10%	197.6 ± 0.8	4.8	11.8 ± 0.1	95.2
pH = 9, 10%	36.5 ± 0.4	3.4	5.1 ± 0.1	96.6
pH = 9, 4%	31.9 ± 0.2	9.1	5.8 ± 0.1	90.9
pH = 9, 1%	92.3 ± 0.1	5.8	26.0 ± 0.1	94.2

[a] τ_1 and τ_2 are longer and shorter decay time constants of Er^{3+}, and R_1 and R_2 are their corresponding contributions.

reports.[28] The variation of lifetime on Yb^{3+} concentration can be mainly attributed to the cross relxations between Yb^{3+} and Er^{3+} and possible back energy transfer from Er^{3+} and Yb^{3+}, which depopulate the green level $^2H_{11/2}/^4S_{3/2}$ largely[9],.[29] According to our previous results: in nanomaterials, the luminescence centers have two positions:[30−34] the surface site locating at or near the surface of nanoparitcles corresponding to the shorter lifetime due to its relative disorder surroundings and the inner site locating in the inner of the nanoparitcles corresponding to the longer lifetime due to its relative order surroundings. However, the present sizes of the nanocrystals are as large as 100 nm, for all the samples. The contribution of surface sites perhaps is not as obvious as those in the nanocrystals smaller than 20 nm. The other possibility has to be considered, that is, the Yb^{3+} ions substitute for two locations, Pb^{2+} or W^{6+}.

D. Local Thermal Effect. For Er^{3+} ions, the energy separation between the nearest excited states $^2H_{11/2}$ and $^4S_{3/2}$ is only several hundred wavenumbers, and the population distribution on $^2H_{11/2}$ and $^4S_{3/2}$ should be dominated by the thermal distribution. Thus, the intensity ratio of $^2H_{11/2}\rightarrow{}^4I_{15/2}$ to $^4S_{3/2}\rightarrow{}^4I_{15/2}$, R_{HS}, is very sensitive to local temperature. Elevated temperature leads to rapid increase of R_{HS}. In UC of Yb^{3+} and Er^{3+} co-doped nanocrystalline systems, when the Yb^{3+} ion concentration and the excitation power were high enough, more 978-nm photons were absorbed. Some of IR light energy inevitably transfers to thermal energy, leading to the temperature increase at the irradiated spot. Here, we use the variation of R_{HS} to analyze the temperature change in UC luminescence processes.

Figure 6a shows the R_{HS} as a function of excitation power and starting Yb^{3+} concentration. It can be seen that, experimentally, R_{HS} increased with the increase of excitation power and Yb^{3+} concentration. Now, let us theoretically consider the variation of temperature on excitation powder density and Yb^{3+} concentration. The intensity ratio of R_{HS}, which is proportional to the population ratio of $^2H_{11/2}$ and $^4S_{3/2}$, should be dominated by Boltzmann's distribution; thus, we have

$$R_{HS} = R_{HS}(0)\exp(-\Delta E/kT) \quad (4)$$

where $R_{HS}(0)$ is a constant, ΔE is the energy separation between the $^2H_{11/2}$ and the $^4S_{3/2}$ levels (~700 cm^{-1}), k is Boltzmann's constant, and T is the absolute temperature. Under the 978-nm laser diode excitation, the temperature at the irradiated spot will increase. It is reasonable to assume that the temperature increase at the irradiated spot is proportional to the adsorbed IR photon energy (power density)

$$\Delta T = \alpha I \quad (5)$$

where α (K mm^2/W) is a constant and I is the power density. The practical temperature at the irradiated spot is

$$T = \alpha I + \beta \quad (6)$$

where β is a temperature constant. On the basis of eqs 4 and 6,

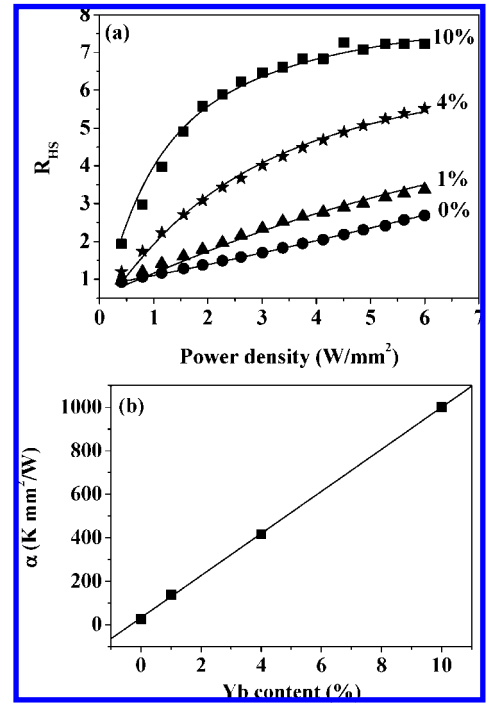

Figure 6. (a) Relationship of R_{HS} and I; scattered dots are experimental data, and solid lines are fitting lines. (b) Relationship of α and Yb content; the scattered dots are the values from Table 3. The solid line is the fitting line.

TABLE 3: Fitting Parameters from Eq 1 in Different Samples

samples	α (K mm^2/W)	$R_{HS}(0)$
10%	1000.1	8.60
4%	416.5	7.77
1%	137.9	8.01
0%	27.3	23.3

R_{HS} as a function of excitation power density can be expressed as

$$R_{HS} = R_{HS}(0)\exp[-\Delta E/k(\alpha I + \beta)] \quad (7)$$

As the excitation power is 0, the sample temperature is room temperature; thus, we can deduce that β = 300 K. In Figure 6a, the experimental dots are well fitted by eq 7. It can be seen that the fitting results using eq 7 are well consistent with the experimental results; the fitting parameters α and $R_{HS}(0)$ are listed in table 3. From Table 3, α increases with Yb concentration. It is natural that the greater the Yb^{3+} concentration is, the more photon energy that is adsorbed and the more the temperature is increased. Figure 6b gives the relation of α and Yb content; it is obvious that they have a linear relationship

$$\alpha = A + BC_{Yb} \quad (8)$$

where C_{Yb} is the content of Yb and A (K mm^2/W) and B (K mm^2/W mol^{-1}) are constants. A is related to the $^4I_{15/2}-{}^4I_{11/2}$ ground-state absorption of Er^{3+} ions. By fitting, the parameters A and B were obtained to be 32.9 (K mm^2/W) and 96.7 (K mm^2/W mol^{-1}), respectively. So the relationship of the temperature of the samples and the Yb content can be expressed as

$$T(K) = (96.7C_{Yb} + 32.9)I + 300 \quad (9)$$

Using this formula, the temperature of the sample at the irradiated spot once the content of Yb and the power density of the excitation laser are determined can easily be obtained. It

should be noted that it is not difficult to understand why in the pH = 9 sample R_{HS} is larger than that in the pH = 4 sample, as mentioned above. The former sample contains much Yb^{3+} content, while the latter contains less.

IV. Conclusions

$PbWO_4:Er^{3+}$, Yb^{3+} nanocrystals were obtained by the hydrothermal method at different pH values (pH = 4, 7, and 9) and their UC luminescence properties were studied. The results indicate that Pb is superfluous relative to W in the hydrothermal products and the increased pH value leads to improved Pb content relative to W and more doping concentration of Yb^{3+}. The relationship between R_{HS} and I was well-fitted assuming the temperature increase at the irradiated spot is proportional to the excitation power density. The fitting parameters also demonstrate that the temperature increase at the irradiated spot depends linearly on Yb^{3+} concentration. The green emissions for Er^{3+} decay biexponentially, suggesting that two luminescent sites of Er^{3+} exist in the $PbWO_4:Yb^{3+}$, Er^{3+} nanocrystals.

Acknowledgment. This work is supported by the National Nature Science Foundation of China (Grants 10704073, 50772042 and 10504030) and the 863 project of China (2007AA032314).

References and Notes

(1) Johnson, L. F.; Geusic, J. E.; Guggenheim, H. J.; Kushida, T.; Singh, S. *Appl. Phys. Lett.* **1963**, *15*, 48.
(2) Kano, T.; Yamamoto, H.; Otomo, Y. *J. Electrochem. Soc.* **1973**, *119*, 1561.
(3) Takahashi, M.; Lzuki, M.; Kanno, F.; Kawamoto, Y. *J. Appl. Phys.* **1998**, *83*, 3920.
(4) Zhou, J.; Moshary, F.; Gross, B. M.; Aark, M. F.; Ahmed, G. A. *J. Appl. Phys.* **2004**, *96*, 237.
(5) Gercia, A. S.; Serna, R.; Castrc, M. J.; Afonso, C. N. *Appl. Phys. Lett.* **2004**, *84*, 2151.
(6) Lei, Y.; Song, H.; Yang, L.; Yu, L.; Liu, Z.; Pan, G.; Bai, X.; Fan, L. *J. Chem. Phys.* **2005**, *123*, 174710.
(7) Bai, X.; Song, H.; Pan, G.; Lei, Y.; Wang, T.; Ren, X.; Lu, S.; Dong, B.; Dai, Q.; Fan, L. *J. Phys. Chem. C* **2007**, *111*, 13611.
(8) Capobianco, J. A.; Vetrone, F.; Alesio, T. D.; Tessari, G.; Speghini, A.; Bettinelli, M. *Phys. Chem. Chem. Phys.* **2000**, *2*, 3203.
(9) Vetrone, F.; Boyer, J. C.; Capobianco, J. A. *J. Appl. Phys.* **2004**, *96*, 661.
(10) Lopez-Luke, T.; De la Rosa, E.; Salas, P. *J. Phys. Chem. C* **2007**, *111*, 17110.
(11) Xu, L.; Yu, N.; Li, G. *Opt. Mater.* **2008**, *30*, 1284.
(12) Chen, Y.; Liu, C.; Somesfalean, G. *Appl. Phys. Lett.* **2008**, *92*, 113114.
(13) Liu, H. Q.; Wang, L. L.; Chen, S. G. *Mater. Lett.* **2007**, *61*, 3629.
(14) Bardelli, L.; Bini, M.; Bizzeti, P. *Nucl. Instrum. Meth. A* **2006**, *569*, 743.
(15) Uitert, L.; Preziosi, S. *J. Appl. Phys.* **1962**, *33*, 2908.
(16) Wang, H.; Medina, F.; Zhou, Y.; Zhang, Q. *Phys. Rev. B* **1992**, *45*, 10356.
(17) Tanaka, K.; Miyajima, T.; Shirai, N.; Zhang, Q.; Nakata, R. *J. Appl. Phys.* **1995**, *77*, 6581.
(18) Lou, Z.; Hao, J.; Cocivera, M. *J. Lumin.* **2002**, *99*, 349.
(19) Kobayashi, M.; Ishii, M.; Usuki, Y. *Nucl. Instrum. Meth. A.* **1998**, *406*, 442.
(20) Hara, K.; Ishii, M.; Kobayashi, M.; Nikl, M.; Takano, H.; Tanaka, M.; Tanji, K.; Usuki, Y. *Nucl. Instrum. Meth A* **1998**, *414*, 325.
(21) Huang, Y.; Seo, H.; Yang, Y.; Zhang, J. *Mater. Chem. Phys.* **2005**, *91*, 424.
(22) Gadsden, J. A. *Infrared Spectra of Minerals and Related Inorganic Compounds*; Butterworth: London, 1975; p 153.
(23) Li, W.; Tang, T. B.; Feng, X. *J. Appl. Phys.* **2000**, *87*, 7692.
(24) Meyssamy, H.; Riwotzki, K. *Adv. Mater.* **1999**, *11*, 840.
(25) Huang, Y.; Seo, H.; Feng, Q.; Yuan, S. *Mater. Sci. Eng.:B* **2005**, *121*, 103.
(26) Song, H.; Sun, B.; Wang, T.; Lu, S.; Yang, L.; Chen, B.; Wang, X.; Kong, X. *Solid State Commun.* **2004**, *132*, 409.
(27) Henderson, B.; Imbusch, G. F. *Optical Spectroscopy of Inorganic Solids*; Oxford University Press: New York, 2006.
(28) Song, H.; Xia, H.; Sun, B.; Lu, S.; Liu, Z.; Yu, L. *Chin. Phys. Lett.* **2006**, *23*, 474.
(29) Vetrone, F.; Boyer, J. C.; Capobianco, J. A.; Speghini, A.; Bettinelli, M. *J. Phys. Chem. B* **2003**, *107*, 1107.
(30) Dai, Q.; Song, H.; Pan, G.; Bai, X.; Zhang, H.; Qin, R.; Hu, L.; Zhao, H.; Lu, S.; Ren, X. *J. Appl. Phys.* **2007**, *102*, 054311.
(31) Bai, X.; Song, H.; Pan, G.; Liu, Z.; Lu, S.; Di, W.; Ren, X.; Lei, Y.; Dai, Q.; Fan, L. *Appl. Phys. Lett.* **2004**, *88*, 143104.
(32) Peng, H.; Song, H.; Chen, B.; Lu, S.; Huang, S. *Chem. Phys. Lett.* **2003**, *370*, 485.
(33) Dai, Q.; Song, H.; Bai, X.; Pan, G.; Lu, S.; Wang, T.; Ren, X.; Zhao, H. *J. Phys. Chem. C* **2007**, *111*, 7586.
(34) Pan, G.; Song, H.; Bai, X.; Liu, Z.; Yu, H.; Di, W.; Li, S.; Fan, L.; Ren, X.; Lu, S. *Chem. Mater.* **2006**, *18*, 4526.

JP805587Q